

Resonant Column Tests and Nonlinear Elasticity in Simulated Rocks

Resmi Sebastian¹ · T. G. Sitharam¹

Received: 8 February 2017 / Accepted: 27 August 2017 / Published online: 5 September 2017
© Springer-Verlag GmbH Austria 2017

Abstract Rocks are generally regarded as linearly elastic even though the manifestations of nonlinearity are prominent. The variations of elastic constants with varying strain levels and stress conditions, disagreement between static and dynamic moduli, etc., are some of the examples of nonlinear elasticity in rocks. The grain-to-grain contact, presence of pores and joints along with other compliant features induce the nonlinear behavior in rocks. The nonlinear elastic behavior of rocks is demonstrated through resonant column tests and numerical simulations in this paper. Resonant column tests on intact and jointed gypsum samples across varying strain levels have been performed in laboratory and using numerical simulations. The paper shows the application of resonant column apparatus to obtain the wave velocities of stiff samples at various strain levels under long wavelength condition, after performing checks and incorporating corrections to the obtained resonant frequencies. The numerical simulation and validation of the resonant column tests using distinct element method are presented. The stiffness reductions of testing samples under torsional and flexural vibrations with increasing strain levels have been analyzed. The nonlinear elastic behavior of rocks is reflected in the results, which is enhanced by the presence of joints. The significance of joint orientation and influence of joint spacing during wave propagation have also been assessed and presented using

the numerical simulations. It has been found that rock joints also exhibit nonlinear behavior within the elastic limit.

Keywords Resonant column apparatus · Wave velocity · Strain levels · Nonlinear elasticity · Resonant frequency · Numerical simulation

List of symbols

V_s	Shear wave velocity
f	Natural frequency of sample
l	Length of specimen
G	Shear modulus
ρ	Density of material
ω_f	Natural flexural circular frequency
E	Young's modulus
I_b	Area moment of inertia
V_{rod}	Compression wave velocity in bounded medium
V_p	Body P wave velocity
m	Mass of specimen
ν	Poisson's ratio
λ	Wavelength of propagating wave
L	Joint spacing
E_m	Rock mass modulus
E_i	Intact rock modulus
k_n	Normal stiffness of joint
k_s	Shear stiffness of joint

✉ Resmi Sebastian
resmisebastian@gmail.com

T. G. Sitharam
sitharam@civil.iisc.ernet.in

¹ Geotechnical Engineering Division, Department of Civil Engineering, Indian Institute of Science, Bangalore 560012, India

1 Introduction

Rocks are generally treated as linear elastic due to simplicity in analysis and calculations even though it is nonlinear elastic. Although rocks exhibit properties of nonlinear elasticity, the studies on the subject are not very

common in the domain of rock mechanics. Rocks disobey the Hook's condition and the hypothesis of continuum, which are the criteria for a linear elastic solid. The dependence of elastic properties on stress and strain, disagreement between static and dynamic moduli, change in wave propagation velocity with changes in confining pressure and curved stress strain behavior on uniaxial testing are classical examples of nonlinearity in rocks. It is regarded that nonlinear theory is relevant for large amplitude vibrations such as shock wave propagations, whereas in fact, nonlinearity is involved in even stress-dependent elastic wave propagation (Liu 1994). Johnson and Rasolofosaon (1996) conducted wave propagation experiments, resonant bar experiments, torsional oscillator experiments and static stress strain tests and established that manifestations of nonlinear behavior occur over the wide strain range of 10^{-9} to 10^{-1} . Bonner and Wanamaker (1990) concluded that well-defined nonlinear effects are noted in soils and rocks at strain levels as low as 10^{-6} . The researchers have found that nonlinearity in rocks and energy dissipation are induced by the presence of pores, grain-to-grain contacts, low aspect ratio cracks, etc. (Johnson and Rasolofosaon 1996; Barton 2007). Presence of discontinuities such as joints and faults and fluids enhance this behavior and make the medium heterogeneous and anisotropic. The rock joints play a significant role in wave propagation through rock mass and wave velocities and wave amplitudes are influenced by the properties of rock and the joints. Elastic constants calculated from the wave velocities obtained within the elastic limit are useful for the analysis and design of structures constructed in them. These calculations are, however, based on the assumption that material is homogenous, isotropic and linearly elastic. However, the piecewise linear approximation to nonlinearity provides satisfactory results.

The experimental studies on wave propagation are centered on the evaluation of wave velocities at a particular strain level. Travel time methods and resonance frequency methods are usually used to obtain wave velocities across rocks (Siggins 1993) and to evaluate the elastic constants. Fratta and Santamarina (2002) and Cha et al. (2009) developed a device to obtain the wave velocities from the resonant frequencies of the rock columns under long wavelength condition. Long wavelength propagation across natural fractures with various joint roughness coefficients was performed by Mohd-Nordin et al. (2014) using quasi-static resonant column test, employing a scan-line technique to analyze the joint fractures. When the wavelength of propagating wave is much longer than joint spacing, it is referred to as long wavelength condition (Fratta and Santamarina 2002). Simulating a long wavelength condition in laboratory is difficult as long column specimens are usually required. Long wavelength condition

is a very general condition in seismology (Cha et al. 2009; Schoenberg and Muir 1989; Schoenberg and Sayers 1995) and hence, an important one. For the usual range of wave frequency associated with earthquakes and the general joint spacing, long wavelength condition is prominent.

A resonant column apparatus is widely used to obtain the low strain dynamic properties of geomaterials, but has some restrictions on the stiffness of testing materials. This usually limits the application of the apparatus in rock mechanics studies. After checking the potential stiffness conditions and also by incorporating some corrections to the obtained resonant frequencies, a study on the dynamic properties of jointed rocks has been conducted by few researchers (Perino 2011; Sebastian and Sitharam 2015, 2016). Perino and Barla (2015) developed a numerical model of the resonant column apparatus to assess the correction factors that are to be applied to the experimental results obtained from laboratory under torsional vibrations, to calculate the actual resonant frequencies. But the previous work on rocks using resonant column apparatus and numerical simulations are restricted to a particular strain level. This paper presents the resonant column tests on intact and jointed samples at various strain levels, thereby examining the nonlinear behavior of rocks within the elastic limit. The numerical simulation of resonant column apparatus, which can provide the resonant frequencies of intact and jointed stiff samples under torsional and flexural vibrations for the long wavelength condition, has also been performed using distinct element method. The model has then been used to analyze the varying stiffness of samples with varying strain levels and joint orientations, by comparing the resonant frequencies obtained from laboratory experiments and numerical simulations. The nonlinear behavior of joint stiffness under torsional and flexural vibrations at three strain levels has also been demonstrated. A study on sample with multiple parallel joints has also been conducted, and results have been presented.

2 Laboratory Experiments Using Resonant Column Apparatus

The resonant column laboratory experiments were conducted on a model material, hardened plaster of Paris (POP) samples (gypsum) of dimensions 50 mm diameter and 100 mm height. The samples were prepared by pouring plaster of Paris—water mix into a prefabricated split mold and drying the set samples under normal humid and room temperatures till they attained a constant weight. The POP powder when mixed with water reforms to gypsum, a common mineral and rock. The uniaxial compressive strength (UCS) of the prepared intact sample (4.165 MPa)

shows that the sample belongs to the class of ‘very weak rock’ (Grade R1) as per the classification of intact rocks by ISRM (1978). The prepared gypsum plaster samples were of density 1070 kg/m³, cohesion of 0.5 MPa, angle of friction 65°, Young’s modulus of 4.5 GPa and Poisson’s ratio of 0.29. Joints (Joint Roughness Coefficient, JRC = 8–10) were introduced into the hardened samples with the help of a fabricated cutter, having two blades, to cut from bottom and top. Resonant column tests were conducted on POP samples with varying number of horizontal joints (one, two, three and four) (Sebastian and Sitharam 2016) and with joints of varying orientations (Sebastian and Sitharam 2015).

In a resonant column test, the seismic wave velocities (*P* and *S*) are calculated from the resonant frequencies of the testing samples, which are obtained from torsional or flexural vibrations. For performing the test, a sample is vibrated in its fundamental mode of vibration. Resonant frequency of the sample is measured after establishing its fundamental mode. The RCA used for the tests has the boundary conditions, bottom fixed and top free with additional masses (driving mechanism) placed on the free end. The electromagnetic drive system consists of magnets surrounded by coils, which are joined to the four arms of rotor (Fig. 1a). For conducting a resonant column test, a sinusoidal excitation is applied to the free end of the sample via the electromagnetic drive system. During torsional tests, the four sets of magnets and coils are connected in series and a net torque is applied to the top of sample during excitation. For conducting flexural tests, two alternate coils surrounding the magnets are switched off, such that a horizontal force is applied to the top of sample when excited. Resonant frequency is evaluated by varying the frequency of applied vibration, and selecting the frequency that induces maximum strains in the sample (by means of an accelerometer that is attached to the driving plate) for that particular amplitude of vibration. A typical resonant frequency curve is shown in Fig. 1b. The voltage measured by the accelerometer is converted to the corresponding strain and is shown by the software attached to the apparatus. By altering the amplitude of vibrations applied to the sample, resonant frequencies at various strain levels can be obtained. The propagations of shear waves in columns are not affected by geometric dispersion (Kolsky 1963). The differentiation of one-dimensional wave equation for shear waves with respect to other two dimensions gives the same shear wave velocity as that with one-dimensional wave propagation. Therefore, the wave velocity obtained using one-dimensional equation is directly applicable to infinite media. The shear wave velocity of the testing material can be calculated from the resonant frequency under torsional vibrations (Richart et al. 1970) as:

$$V_s = \frac{2\pi fl}{\beta} \tag{1}$$

where *f* natural frequency of the sample obtained from resonant column test, *l* length of sample, *V_s* shear wave velocity and, $\beta = I_0 \tan \beta$, where *I* is the mass polar moment inertia of the sample and *I₀* is the mass polar moment inertia of the drive system.

The shear modulus of the material is obtained as:

$$G = \rho V_s^2 \tag{2}$$

Kolsky (1963) presented a method for measuring Young’s modulus from the resonant frequencies obtained under flexural vibrations. The whole system involving the specimen and driving system is considered elastic, as a lumped mass at the end of specimen. This can be represented as a cantilever beam with a horizontal load at the free end, which has a linearly varying displaced shape along the longitudinal axis. It is considered that the total energy of the system remains constant as it is elastic. The theory behind application of flexural vibrations using RCA can be explained using Rayleigh’s energy method. The compression wave velocity in a bounded medium can be calculated from the Young’s modulus of sample, then. Using Rayleigh’s method, Young’s modulus is obtained from the natural circular frequency of sample (Cascante et al. 1998) as:

$$\omega_f^2 = \frac{3EI_b}{\left[\frac{33}{140}m + \sum_{i=1}^n m_i h(h_{0i}, h_{1i})\right]l^3} \tag{3}$$

where ω_f natural flexural circular frequency of sample, *E* Young’s modulus, *I_b* area moment of inertia (second moment of area) of the sample, *m* mass of the sample, *m_i* mass of each additional mass placed on top of sample such as top cap, top plate, driving plate. (*i* = 1, 2, ...)

$$h(h_{0i}, h_{1i}) = 1 + 3 \frac{(h_{0i} + h_{1i})}{2l} + \frac{3}{4} \left(\frac{h_{0i}^2 + h_{1i}h_{0i} + h_{1i}^2}{l^2} \right)$$

where *h_{0i}* the distance measured from the top of sample to the bottom of additional mass *m_i*, *h_{1i}* the distance measured from the top of sample to the top of additional mass *m_i*.

The longitudinal or compression wave velocity in a bounded medium is obtained as:

$$V_{rod} = \sqrt{\frac{E}{\rho}} \tag{4}$$

where ρ is the density of material.

The body P wave velocity *V_p* is obtained from *V_{rod}* as,

$$V_p = V_{rod} \sqrt{\frac{(1 - \nu)}{(1 + \nu)(1 - 2\nu)}} \tag{5}$$

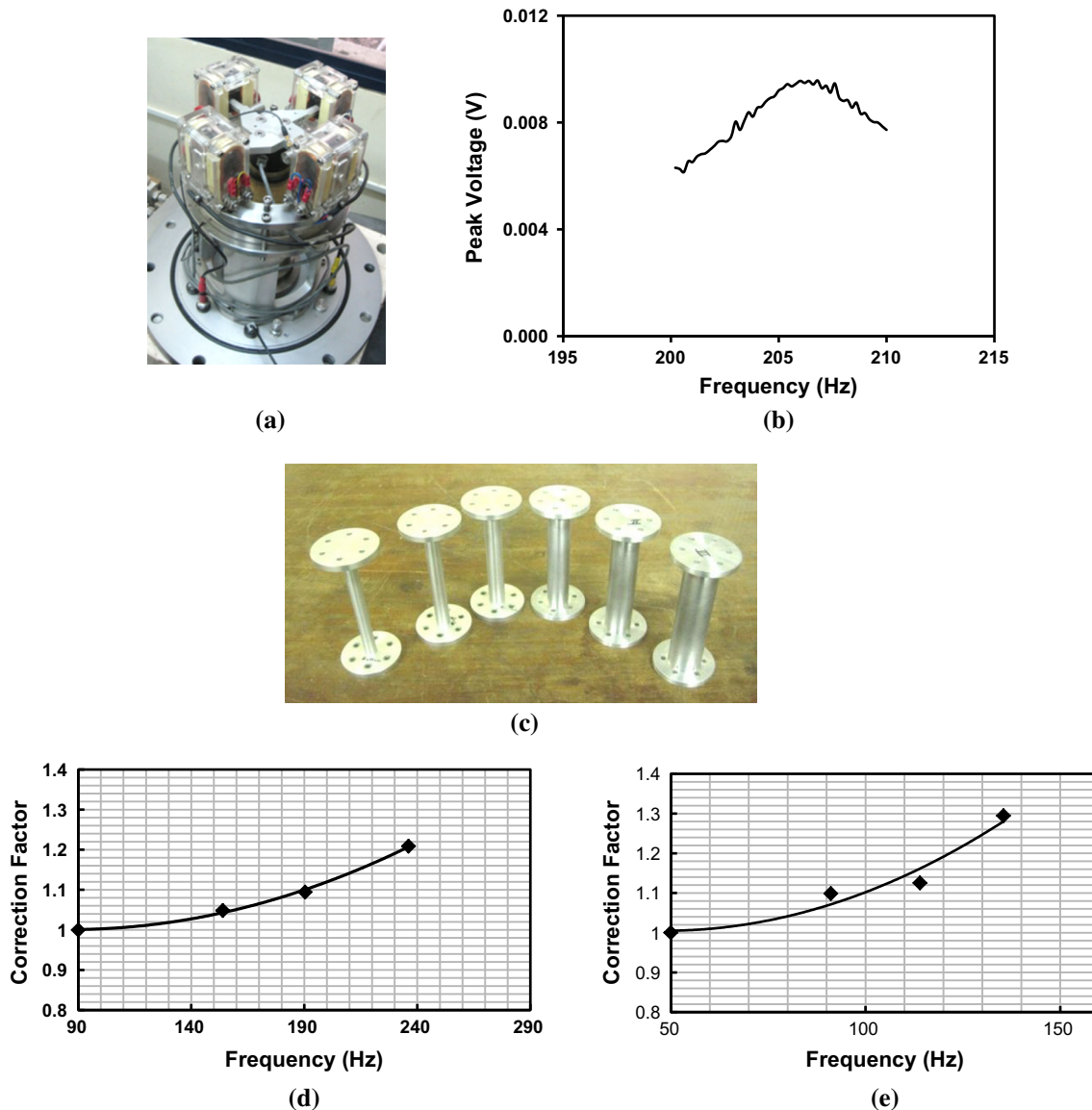


Fig. 1 **a** Resonant column apparatus, **b** a typical resonant frequency curve, **c** calibration bars used for obtaining corrections, **d** corrections factors for resonant frequencies obtained under torsional vibrations and **e** correction factors for resonant frequencies obtained under flexural vibrations

where ν is the Poisson's ratio of the specimen.

For a rod of finite length, under fixed free boundary condition, the wavelength of propagating wave is four times the length of specimen (rod). For the RCA used for testing, the presence of additional masses (driving mechanism) alters the boundary condition. The wavelength calculated from the wave velocity and resonant frequency attains the long wavelength condition as it is more than ten times the joint spacing. It is also to be noted that the wave velocity obtained under flexural vibrations is the longitudinal or compression wave velocity in a bounded medium. The calculation of body P wave velocity involves the use of Poisson's ratio of specimen, obtained from the wave velocities. The evaluation of Poisson's ratio from wave

velocities is valid when material is homogenous, isotropic and linearly elastic. As a jointed rock sample does not satisfy these conditions (Thomsen 1990, 1996), calculation of body P wave is avoided.

As RCA is designed for evaluating the low strain properties of soils, there are certain problems associated with testing stiff samples using the apparatus. Insufficient coupling of samples with end platens, fixity of bottom pedestal (Drnevich 1978) and over stiffness of samples (Drnevich 1978; Kumar and Clayton 2007) are the usual problems that are expected while obtaining resonant frequencies of stiff samples. The apparatus setup in the laboratory and the sample (prepared using POP) were checked against the various stiffness criteria, and it was found to be

satisfactory within the limits. The usage of less stiff POP samples was advantageous in this regard. Insufficient coupling of samples with end platens leading to the slippage of stiff (POP) samples from the platens during vibrations was solved by applying epoxy resins at the ends of samples, so that they got fixed to end platens (Khan et al. 2008). Even if the stiffness of samples is within the limits, resonant column tests may generate lower natural frequencies than the actual natural frequencies, for stiff samples (Kumar and Clayton 2007). Corrections to the generated resonant frequencies are therefore required to obtain the actual resonant frequencies. Aluminum calibration bars of various diameters (Fig. 1c) were used to calculate the correction factors. The natural frequencies vary depending on their diameters, but standard values of shear and Young's moduli are expected from the resonant frequencies. It was observed that stiff samples (with large diameters) generated lower values than expected. The expected resonant frequencies were calculated from the established moduli values and were compared against obtained resonant frequencies, and ratios were taken. The corrections calculated for the obtained resonant frequencies for stiff samples under torsional and flexural vibrations are shown in Fig. 1d, e. Actual resonant frequencies are determined by multiplying the obtained resonant frequencies with the correction factors.

The wavelength (λ) of the propagating waves calculated from the wave velocities and resonant frequencies (f_s resonant frequency under torsional vibration, f_p resonant frequency under flexural vibration) for samples (sample size 50 mm \times 100 mm) with varying numbers of joints indicated that (Sebastian and Sitharam 2016) they are much longer than the joint spacing, L ($\lambda > 10L$) and attain the long wavelength condition.

3 Resonant Column Tests and Nonlinear Behavior in Rocks

Figure 2a, b shows the shear and compression wave velocity reduction of samples without joint and various numbers of joints. It is observed that the sample without any joint has highest wave velocity and has varying wave velocities with strain levels; clearly depicting the nonlinear behavior, although nearly linear portion is visible at lower strain levels. The nonlinear behavior is observed to increase with increasing number of joints. The dependence of wave velocities on the hydrostatic confining stress and on joint orientations at various strain levels is already shown by Sebastian and Sitharam (2016) and Sebastian and Sitharam (2015). As mentioned earlier, the dependence of wave velocities and elastic constants on strain levels and

applied hydrostatic stresses indicates the nonlinear behavior of intact and jointed rocks.

4 Numerical Simulation of Resonant Column Tests

The numerical simulation of resonant column tests has been performed using 3DEC (3-Dimensional Distinct Element Code) by Itasca Consulting Group Inc. Even though the experiment could be simulated by the direct application of vibration to the sample for easiness, the entire resonant column apparatus was modeled to generate the exact conditions that are experienced by the specimen during testing in laboratory. The numerical model of resonant column apparatus used in the laboratory is shown in Fig. 3a. The blocks of the numerical model, such as testing sample (gypsum plaster samples), driving plate, top plate, top cap, accelerometer and counter weight, were made deformable. For the proper simulation of wave transmission through the model, the size of the finite difference elements should be smaller than 1/8th of the wavelength of propagating wave (Kuhlemeyer and Lysmer 1973), whereas Deng et al. (2012) suggested the size should be smaller than 1/32nd of the wavelength of propagating wave. In consideration of these conditions, the mesh size was selected to be 0.005 m (average edge length of tetrahedral element) and 28,037 elements were used to describe the entire model.

Elastic isotropic model was prescribed for all the materials used in the simulation as the vibrations generated in RCA induce only low strain levels (within the elastic limit) in the materials. As the material POP represents the rock material in present study and rock itself is of dissipative nature (an indication of the nonlinear behavior within elastic limit), the material exhibits frequency-dependent behavior (Barton 2007). As mentioned in introduction, the presence of pores, grain-to-grain contacts, etc., result in nonlinear elasticity of intact rocks. However, the presence of joints and other discontinuities increase the nonlinear behavior of rocks. The changes in wave velocities and moduli with varying strain levels indicate this behavior. Hence the properties of the POP material to be adopted for the specimen were obtained from resonant column tests conducted in laboratory at three strain levels.

The RCA has its boundary conditions as bottom fixed and top free with additional masses at the free end, under torsional and flexural vibrations. The base of the model was fixed by setting the velocities in all directions to be zero. Driving mechanism and other additional masses placed on top of the sample were joined to simulate the connections

Fig. 2 Variations of wave velocity with strain levels
a shear wave velocity,
b compression wave velocity

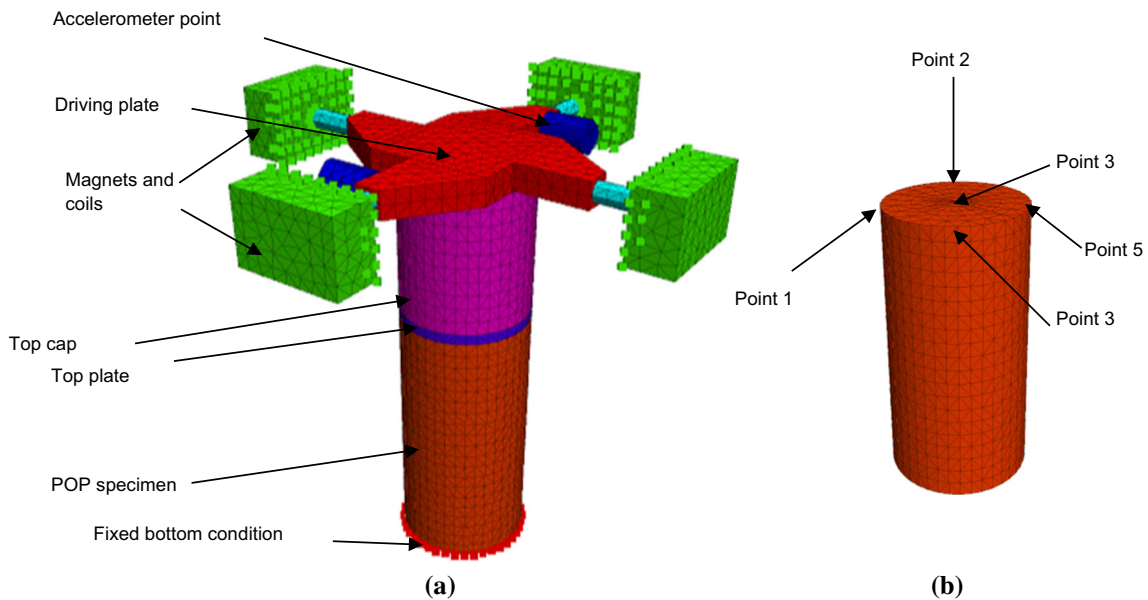
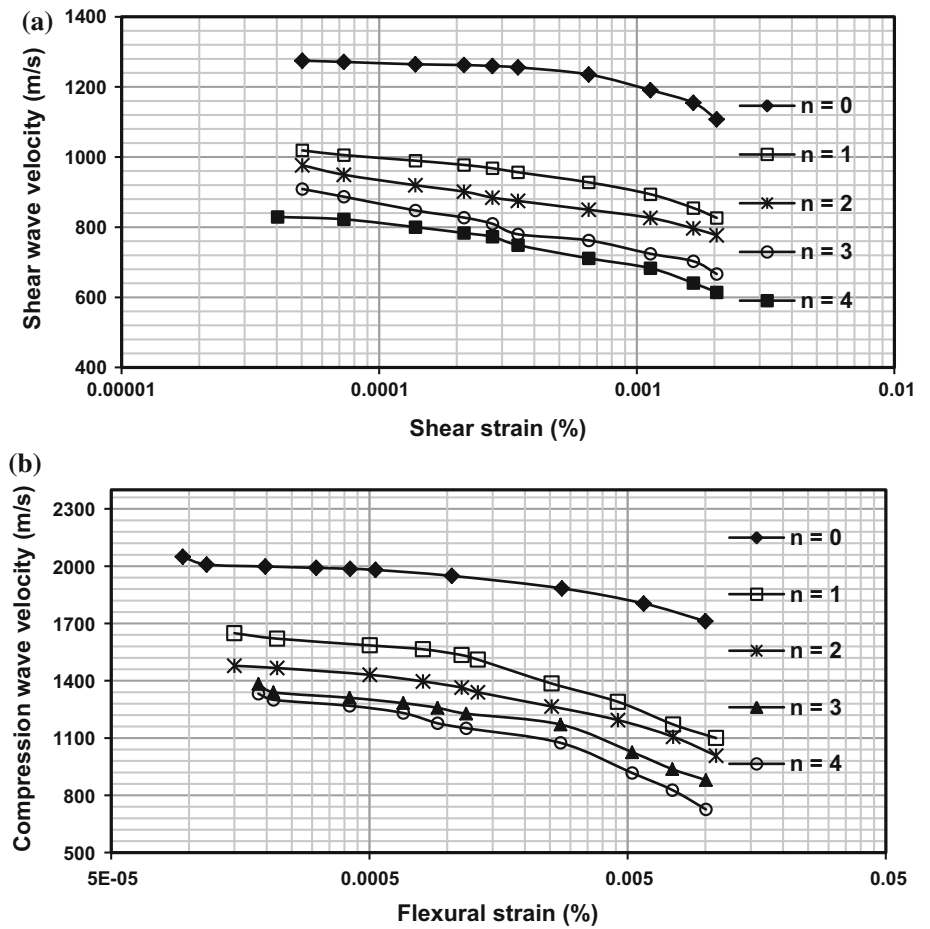


Fig. 3 **a** Numerical simulation of RCA and **b** monitoring points for displacement

that are involved in setting up the sample to perform the experiment. For simulating the torsional vibrations applied to the sample, a sinusoidal stress of appropriate frequency

was prescribed on the inner sides of the four magnets such that a net torque is applied to the top of sample as explained in Sect. 2.

The frequencies of the applied vibrations were varied, and the displacements at the outer edges of the samples were monitored. In the laboratory testing, the accelerometer is usually placed at an offset distance from the sample edge and displacements of samples are calculated by taking into consideration, the offset distance from the axis of rotation. The numerical model provides the flexibility to measure the actual displacements of the sample at any point, and the sample edges were chosen as the monitoring points for obtaining resonant frequencies. The monitoring points of the sample for evaluating the displacements are displayed in Fig. 3b. The frequency for which the sample produced maximum net displacement was considered as the resonant frequency, under a particular strain level, for torsional vibrations. No damping was prescribed to the material, as the resonant frequencies are evaluated using forced vibrations.

For applying flexural vibrations to the sample, sinusoidal stresses were applied on alternate magnets so that a horizontal stress is induced on the top end of sample. The displacements in the direction of movement of sample were monitored for all the applied frequencies to evaluate the resonant frequencies. As the resonant frequencies obtained from numerical model were to be compared against those obtained from laboratory experiments at 100 kPa confining stress, same confining stress was applied to the numerical model.

The shear stress calculated from the shear modulus of the sample and the shear strain developed in the sample were used to obtain the loading applied on the inner side of each magnet. The calculated shear stresses from the laboratory tests could impart torsional vibrations of desired amplitudes, to the sample, such that displacements developed in the sample were comparable to those from laboratory tests. For application of flexural vibrations, the flexural stress calculated from the Young's modulus and the flexural strain were used to obtain the stress (loading) to be applied on the magnets for setting up the vibrations. The numerical simulations and analysis of resonant column tests on intact sample, sample with horizontally aligned single joint, sample with inclined joint and sample with two horizontally aligned joints are described in the following sections.

5 Numerical Simulation of Experiment with Intact Sample

Figure 4a, b shows the intact POP sample used for laboratory testing and the numerical model, respectively. Torsional and flexural vibrations were applied to the sample at three strain levels, and resonant frequencies were obtained. The resonant frequency curves under torsional and flexural

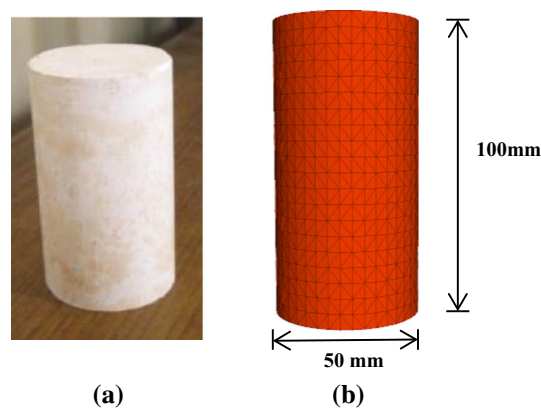


Fig. 4 a Intact POP sample and b numerical model of intact POP sample

vibrations and the resonant frequency reduction curves obtained from the simulations for increasing strain levels are explained in the following sections.

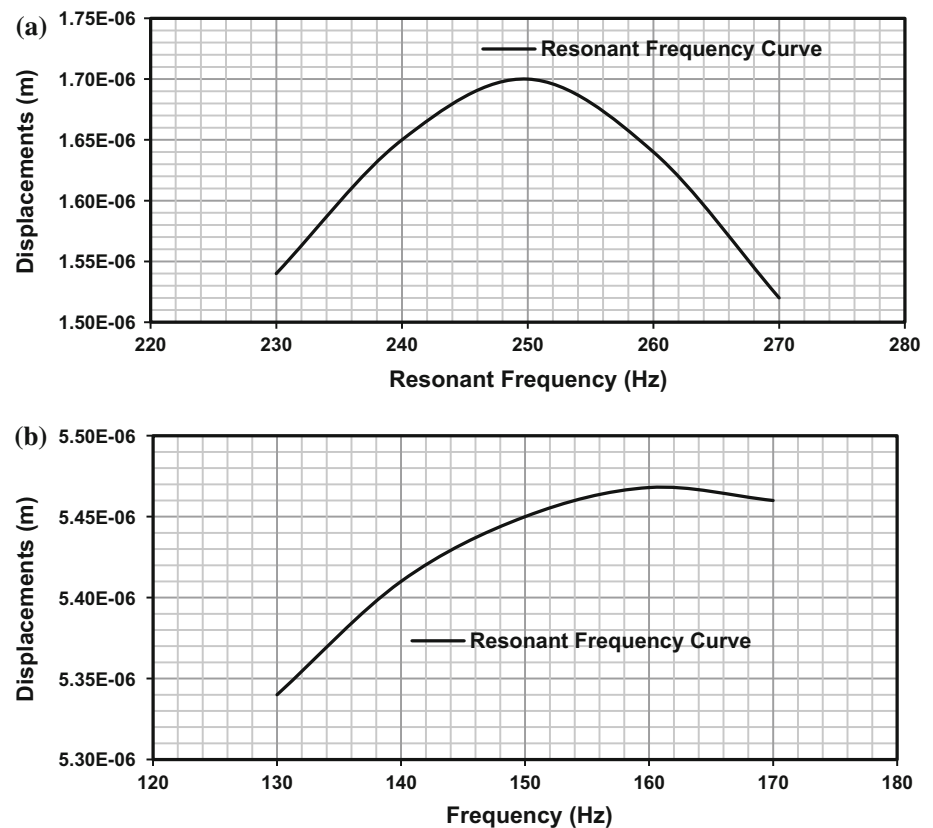
5.1 Resonant Frequency Curves

The shear stresses at three strain levels (obtained at laboratory), $1.7e-4$, $8e-4$ and $2.5e-3\%$, were applied to the magnets in sinusoidal mode at different frequencies, and resonant frequencies were obtained. A typical resonant frequency curve under torsional vibrations (from numerical simulation) at strain $2.5e-3\%$ (obtained at laboratory) is shown in Fig. 5a. Similarly, the resonant frequency curves were obtained at three strain levels ($2e-4$, $1e-3$ and $3.8e-3\%$) under flexural vibrations. Resonant frequency curve at the strain, $3.8e-3\%$, is shown in Fig. 5b. The plots indicate that resonant frequencies were obtained to be 250 and 161 Hz, respectively, under torsional and flexural vibrations (from numerical simulations). The maximum displacements indicated in the figures (for the resonant frequency) correspond to the obtained strain level. For each strain level, the displacements monitored at all monitoring points (shown in Fig. 3b) were same, indicating that same amount of stress was applied by magnets to the sample, simulating well the conditions that existed during laboratory tests.

5.2 Resonant Frequency Reduction Across Strain Levels

Resonant frequencies were evaluated at ten strain levels during laboratory experiments, to calculate the wave velocities. But resonant frequencies were obtained at three strain levels only using numerical simulations as modeling the vibration at each frequency takes considerable time. A comparison of the resonant frequencies obtained from numerical models across various strain levels and those

Fig. 5 Resonant frequency curve for an intact sample **a** under torsional vibrations, **b** under flexural vibrations



obtained from laboratory experiments is shown in Fig. 6. The plots indicate that resonant frequencies get reduced with increasing strain levels and the numerical results are in agreement with the experimental results. As wave velocities are calculated from the resonant frequencies, the figures depicted here indicate the wave velocity reduction and indirectly, the moduli reductions with increasing strain levels. Even though the sample tested is an intact one (without any joint), the material behavior is strain dependent (frequency dependent and amplitude dependent), even within elastic range, and indicates that it is a dissipative medium which is due to the existence of various micro-defects.

6 Selection of Joint Properties for Numerical Model

The Coulomb slip joint criterion, which is the generalization of Coulomb friction law, has been adopted to describe the joint behavior. The behavior of the joint is governed by stiffness of joint within the elastic limit. Joint stiffness, which is an essential parameter in numerical modeling, is not an easily measured one. They are measured in direct shear tests with the help of joint displacement transducers and using strain gauge type extensometer in triaxial shear

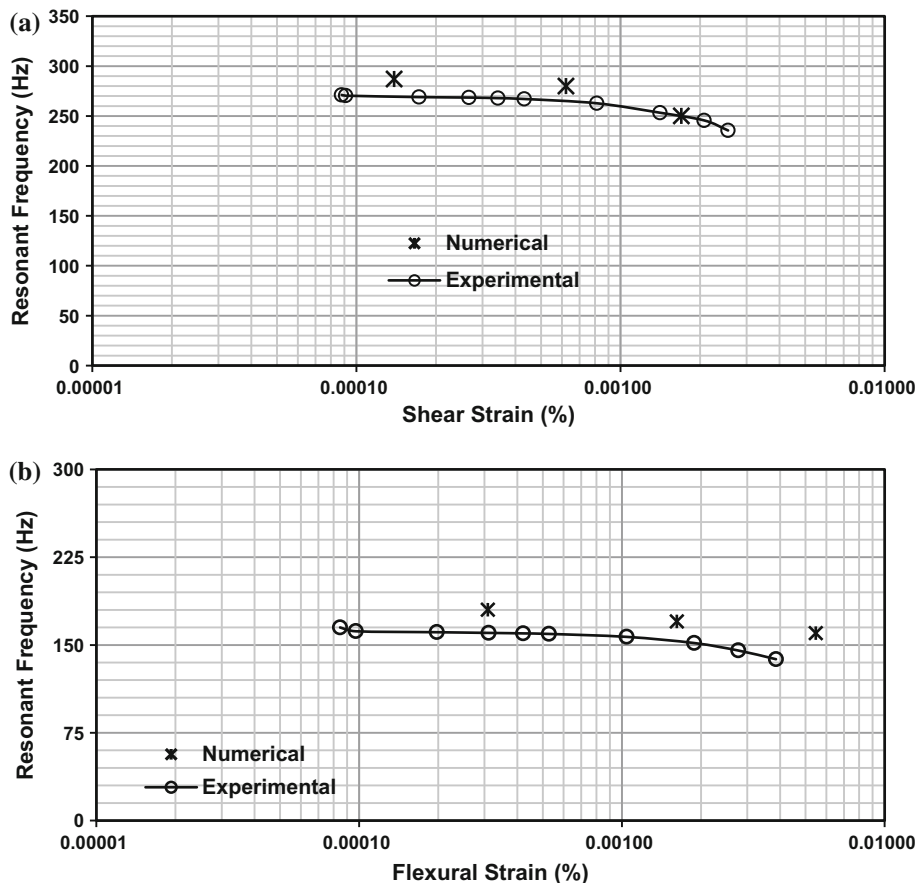
tests (Rosso 1976; Li et al. 2012). Another method to estimate the parameter is based on the deformability of rocks. If it is assumed that deformability of rock mass is the sum of the deformability of intact rock and of the joint, then the joint normal stiffness can be obtained as:

$$\frac{1}{E_m} = \frac{1}{E_i} + \frac{1}{k_n L} \quad (6)$$

where E_m is the rock mass modulus, E_i is the intact rock modulus, k_n is the joint normal stiffness and L is the spacing of joints. Similarly the equation for estimating the joint shear stiffness can also be obtained. But it is to be noted that the equation is applicable for the condition when a single set of joints are present in the rock mass. Moreover, the concept of superposition, based on which the equation is derived, is applicable only for linear elastic solids (Liu 1994). Hence, the equation provides an approximate method to obtain the stiffness of joints. Pande and Orlando (2011) ascertained that stiffness of joint is nonlinear, in contrast to the general assumption in engineering analyses and is dependent on the normal and shear stress on joints.

The normal and shear stiffness of joint at various strain levels within the elastic limit required for the numerical simulation was obtained by numerical trial-and-error simulations. A rough estimate on the joint stiffness was made on the basis of the typical displacement and the stresses

Fig. 6 Resonant frequency reduction across strain levels for intact sample **a** torsional vibrations, **b** flexural vibrations



that were applied to the system. Then a trial-and-error method was followed to obtain the joint stiffness. The displacements were obtained at the joints during numerical simulations and were found to be low values, always within the elastic limit. The range of displacements obtained at the joints during numerical simulations were in the range of strains obtained at joints by Cha et al. (2009) during resonant column tests at laboratory. At each strain level, a particular value of stiffness was assumed for the joint and the resonant frequency obtained from the numerical model was compared against that from laboratory experiment. The joint stiffness that provided comparable resonant frequency with the laboratory value at the particular strain level was selected. The deformational behavior of rock behavior is generally modeled as linearly elastic without any frictional and tensile damages (Cai and Zhao 2000) for elastic wave propagation. Potyondy (1961) and Panchanathan and Ramaswamy (1964) reported that limiting maximum value of interface friction is the peak internal friction angle. Therefore, the properties of intact material (gypsum plaster sample) such as cohesion and angle of internal friction were adopted as the joint cohesion and joint friction angle for numerical simulation. This was done to ensure that frictional damage of the joint does not take place during these vibrations.

Figure 7a, b shows the selection of k_s and k_n at strain levels of $1.18 \times 10^{-4}\%$ and $4.7 \times 10^{-3}\%$, respectively, for the sample with one horizontal joint. At the strain level of $1.7 \times 10^{-4}\%$, the laboratory experiment provided a resonant frequency of 210.5 Hz under torsional vibrations. Figure 7a shows that the numerical model with joint shear stiffness of 2.5×10^9 Pa/m achieved a resonant frequency of 210 Hz at a comparable strain level of $1.18 \times 10^{-4}\%$. Similarly, for flexural vibrations, at the strain level of $2.5 \times 10^{-3}\%$, the laboratory experiment provided a resonant frequency of 112 Hz, whereas the numerical model with normal stiffness of joint, 1×10^{10} Pa/m, presented a resonant frequency of 126 Hz at strain level of $4.7 \times 10^{-3}\%$. A comparison of the resonant frequencies obtained under torsional and flexural vibrations from the numerical simulations and laboratory experiments is shown in Table 1.

7 Numerical Simulation of the Experiment with One Horizontal Joint

The numerical simulation of resonant column experiment on a horizontally jointed sample has been performed by incorporating a joint into the already simulated numerical model. The jointed POP sample and its simulated model

Fig. 7 Selection of joint stiffness **a** shear stiffness, **b** normal stiffness

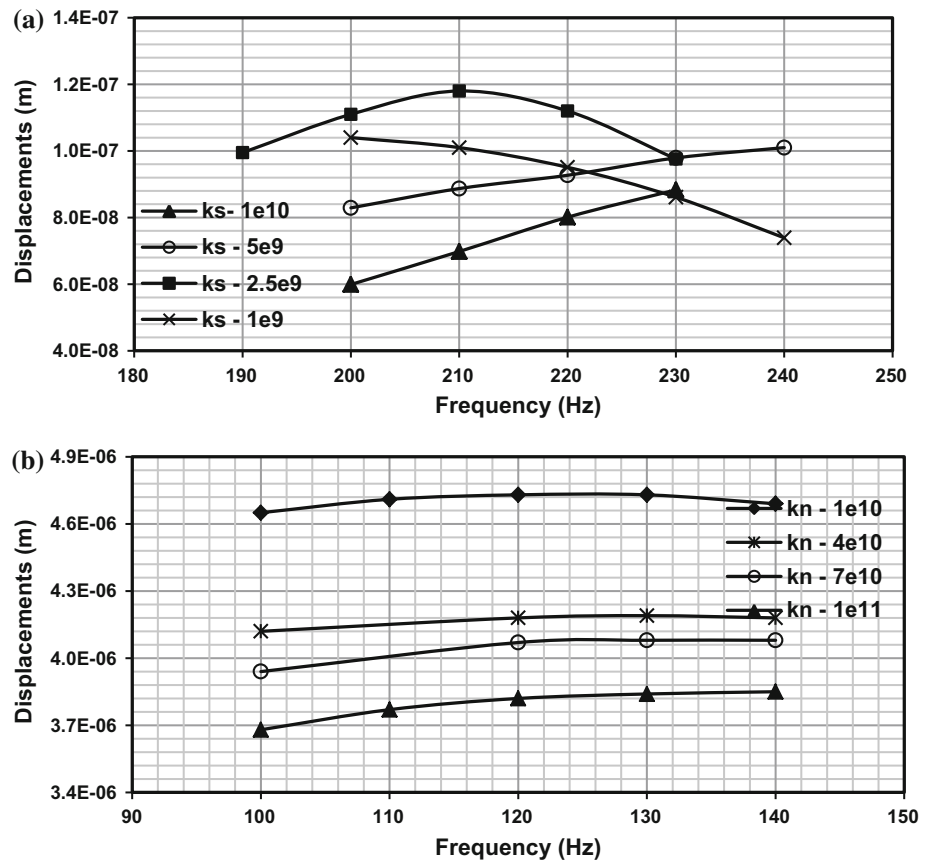


Table 1 Resonant frequencies obtained from laboratory experiments and numerical simulations

Vibration	Numerical results		Experimental results	
	Resonant frequency (Hz)	Strain (%)	Resonant frequency (Hz)	Strain (%)
Torsion	287	1.39e-4	269	1.7e-4
Flexure	180	3e-4	169	2e-4

are shown in Fig. 8a, b. The resonant frequency reductions, joint stiffness and the displacement behavior of joints under torsional and flexural vibrations are discussed in the following sections.

7.1 Resonant Frequency Reduction Across Strain Levels

The resonant frequency reductions with increasing strain levels obtained from numerical model and laboratory experiments are displayed in Fig. 9a, b under torsional and flexural vibrations. The plot shows that numerical results are in agreement with the results obtained experimentally in laboratory. The resonant frequencies obtained were 210, 190 and 166 Hz, respectively, at strain levels, 1.2e-4, 5.6e-4 and 1.72e-3% under torsional vibrations. Similarly, the resonant frequencies were obtained to be 137, 126 and 100 Hz, respectively, at strain levels 9.8e-4, 4.73e-3 and 1.96e-2% under flexural vibrations.

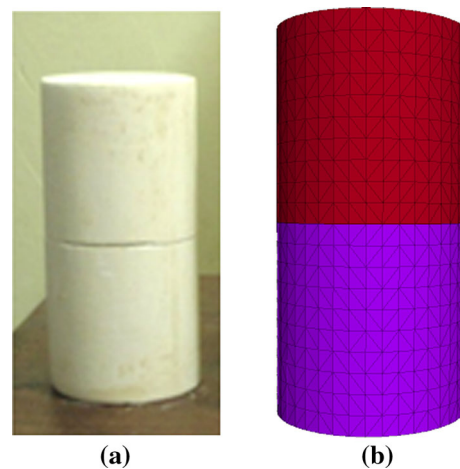
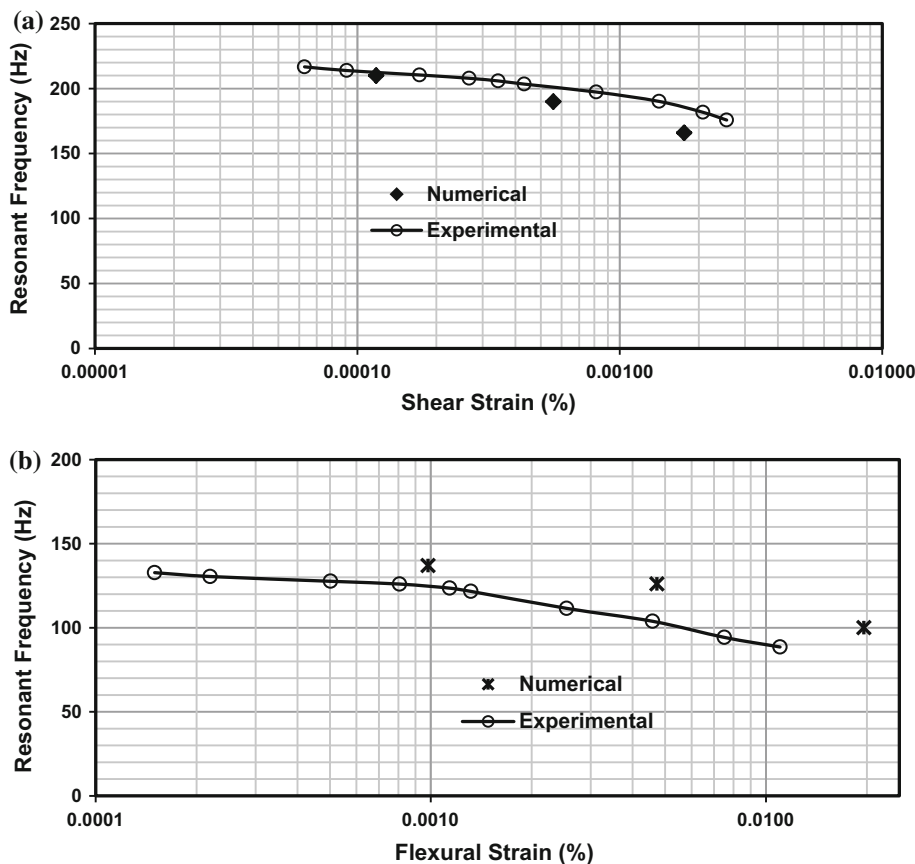


Fig. 8 **a** A jointed POP sample and **b** numerical model of jointed POP sample

Fig. 9 Resonant frequency reductions across strain levels for sample with horizontal joint **a** under torsional vibrations, **b** under flexural vibrations



7.2 Reduction of Joint Stiffness Across Strain Levels

The normal stiffness and shear stiffness of joint at various strain levels used for the numerical simulation of resonant column tests with one horizontal joint are displayed in Fig. 10. As the joint stiffness was calculated such that the resonant frequencies obtained from numerical models matched to those calculated from laboratory experiments, these values provide an idea of stiffness reduction pattern in jointed rocks with increasing strain levels. It is observed that normal stiffness of joint shows a drastic reduction (from $1e11$ Pa/m to $5e9$ Pa/m) as the strain level varies from $9.8e-4$ to $1.9e-2\%$, whereas joint shear stiffness reduces from $2.5e9$ Pa/m to $1e9$ Pa/m as strain level varies from $1.18e-4$ to $1.7e-3\%$. This stiffness reduction of joints leads to reduced resonant frequencies and wave velocities, with increasing strain levels, along with the stiffness reduction of material with increasing strains. Winkler and Nur (1979) established that materials that have potential (micro) sliding surfaces show strain amplitude dependence. Joint shear stiffness shows a mild reduction, but normal stiffness of joint shows a drastic reduction with the observed strain levels. This may be due to the difference in the range of strain levels for which the

joint stiffness was calculated. However, it can be concluded that joint stiffness exhibits nonlinear behavior and shows strain dependence as indicated by Pande and Orlando (2011).

8 Numerical Simulation of Experiment with One Inclined Joint

The behavior of an inclined joint under wave propagation has been studied by numerically simulating the resonant column experiments performed on the sample in laboratory. A POP sample with a joint aligned at 50° orientation and the numerical model developed to simulate the same are displayed in Fig. 11a, b, respectively. The resonant frequency curves under torsional and flexural vibrations as well as the reduction of joint stiffness with increasing strain levels are discussed in the following sections.

8.1 Resonant Frequency Reduction Across Strain Levels

The resonant frequency curves obtained under torsional and flexural vibrations from the numerical models with

Fig. 10 Reduction of joint stiffness for sample with horizontal joint across strain levels

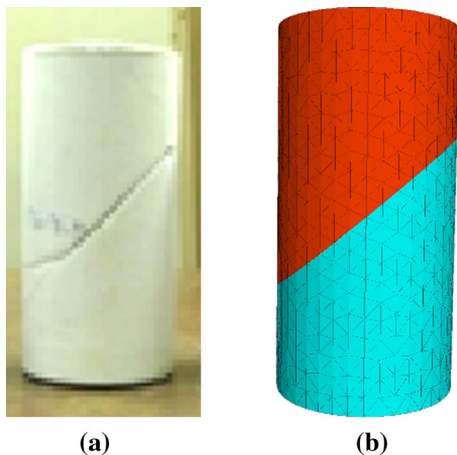
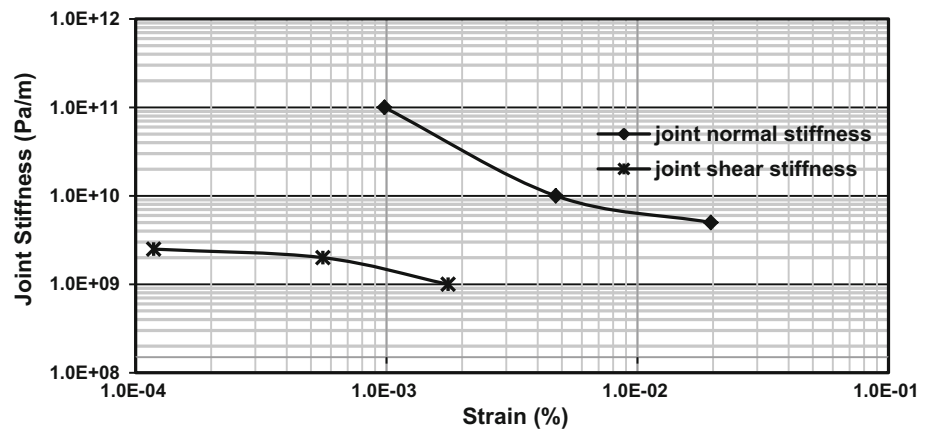


Fig. 11 **a** A POP sample with joint aligned at 50° to the vertical axis and **b** numerical simulation of jointed POP sample

inclined joint at various strain levels are shown in Fig. 12a, b, respectively. The resonant frequencies obtained were 232, 229 and 171 Hz, respectively, for strain levels, $1.3e-3$, $5.2e-3$ and $1.25e-2\%$ under torsional vibrations, whereas the resonant frequencies obtained were 130, 126 and 104 Hz, respectively, for strain levels $1.18e-3$, $4.57e-3$ and $1.44e-2\%$ under flexural vibrations. It is observed that resonant frequencies for the inclined joint at various strain levels are higher than those with the horizontal joint under torsional vibrations, even at higher strain levels.

8.2 Joint Stiffness Reduction Across Strain Levels

Figure 13a, b shows the reductions of normal and shear stiffness with increasing strain levels for various joint orientations. It is observed that the joint stiffness obtained at various strain levels is higher when the joint orientation is 50° than when the joint orientation is 90° (horizontal). This implies that increase in the joint stiffness at inclined orientations is the reason behind the enhanced wave velocities that are observed at laboratory experiments. This

in turn points to the fact that jointed rocks with inclined joints are stiffer than those with horizontal joints.

9 Numerical Simulation of Experiment with Multiple Horizontal Joints

The simulation of resonant column experiments has been extended to samples with multiple joints to validate the developed numerical model. Two horizontal joints were added, and resonant frequencies under torsional and flexural vibrations were obtained at three strain levels. The POP sample with two horizontal joints and the numerical model are shown in Fig. 14a, b. The joint stiffness (k_n and k_s) calculated from the numerical model with one horizontal joint was used to describe the joint behavior. The influence of joints in reducing the wave velocities and stiffness of rock mass is demonstrated in the following sections.

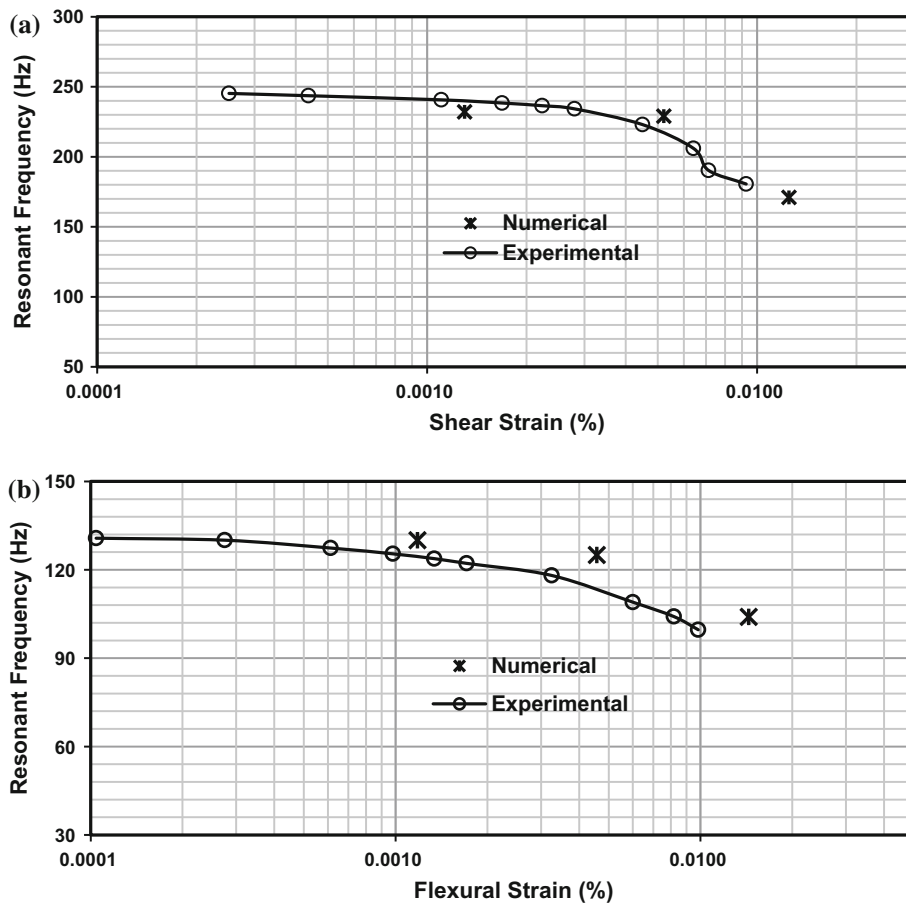
9.1 Resonant Frequency Reduction Across Strain Levels

The resonant frequency reductions under torsional and flexural vibrations with increasing strain levels, acquired from numerical models and laboratory experiments, are displayed in Fig. 15a, b. The plots show that results obtained numerically and experimentally are in good agreement. The resonant frequency curves under torsional and flexural vibrations at different strain levels are given in Sitharam and Resmi (2017).

9.2 Influence of Number of Joints/Joint Spacing

Figure 16a, b shows the resonant frequency reductions obtained from numerical models under torsional and flexural vibrations for various number/spacing of joints. The stiffness reduction of the sample with the introduction of

Fig. 12 Resonant frequency reduction across strain levels for sample with inclined joint under **a** torsional vibrations, **b** flexural vibrations



more joints is clearly visible in both the plots. The resonant frequency reduction with reduction in joint spacing is the indication of moduli reduction, which is also observed with increasing strain levels. The trend is common, both under torsional and flexural vibrations. While the dissipative nature of rocks is responsible for the stiffness reduction of samples with increasing strain levels for intact samples, the presence of more joints adds up to the nonlinear behavior of rocks.

9.3 Vibration of Samples with Multiple Joints

While numerically simulating the resonant column test on sample with multiple joints, it is important to check if the vibrations are transferred across joints or not. This is to ensure that the resonant frequency of the whole sample is obtained from the test rather than that of a portion of sample. For evaluating this condition, vibrations were applied to the sample with four joints (Fig. 17a). The contours of stress and displacements during torsional and flexural vibrations are shown in Fig. 17b–e. The displacement and stress contours under torsional vibrations (Fig. 17b, c, respectively) imply that stresses and

displacements are transferred across the joints indicating the transmission of vibration. The displacement and stress contours under flexural vibrations (Fig. 17d, e) also indicate the same.

10 Wave Velocities from Resonant Frequencies

The wave velocities are calculated from the resonant frequencies at various strain levels using formulae (1) and (4). Table 2 shows the wave velocities calculated at various strain levels from the resonant frequencies obtained using numerical simulations. It is to be noted that longitudinal or compression wave velocity in a bounded medium, calculated from the flexural vibrations, as mentioned in Sect. 2 is presented here.

11 Discussion

The vibrations generated by different sources induce strain levels in various ranges in a rock mass, depending on the type of source and distance of point of interest from the

Fig. 13 Reduction of joint stiffness across strain levels for various joint orientations **a** shear stiffness, **b** normal stiffness

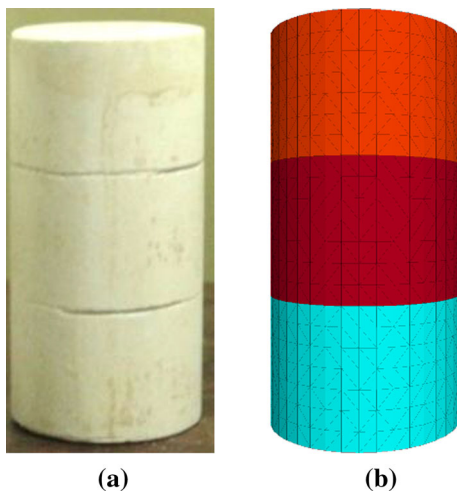
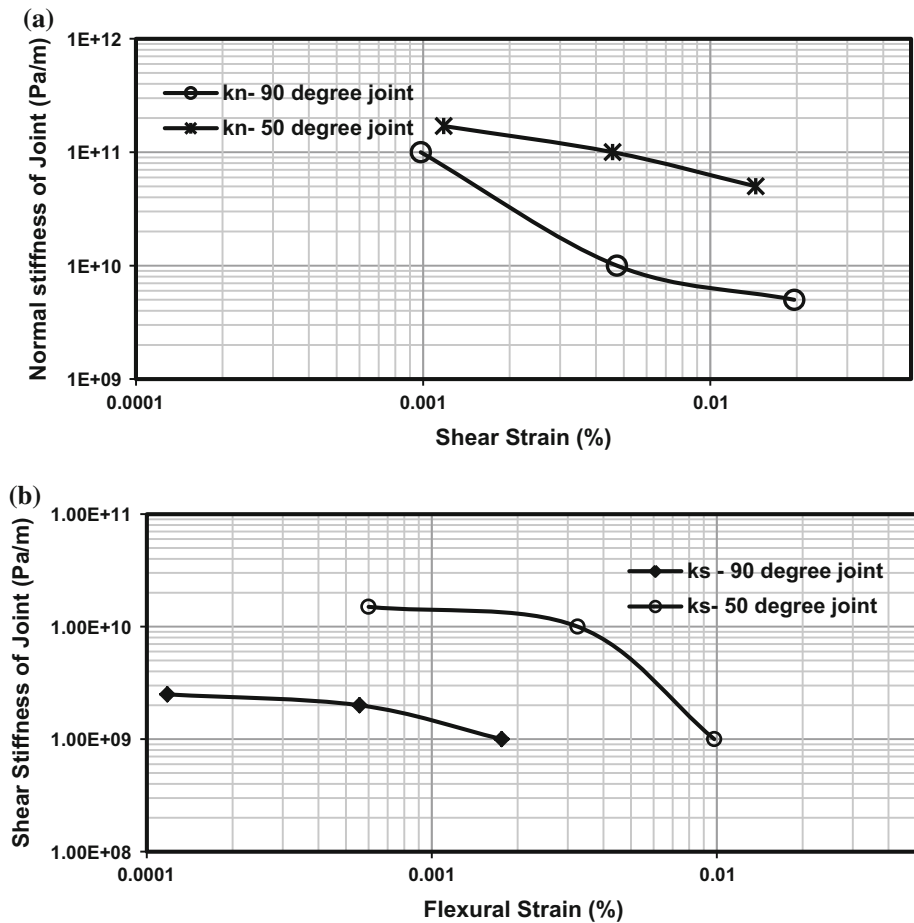


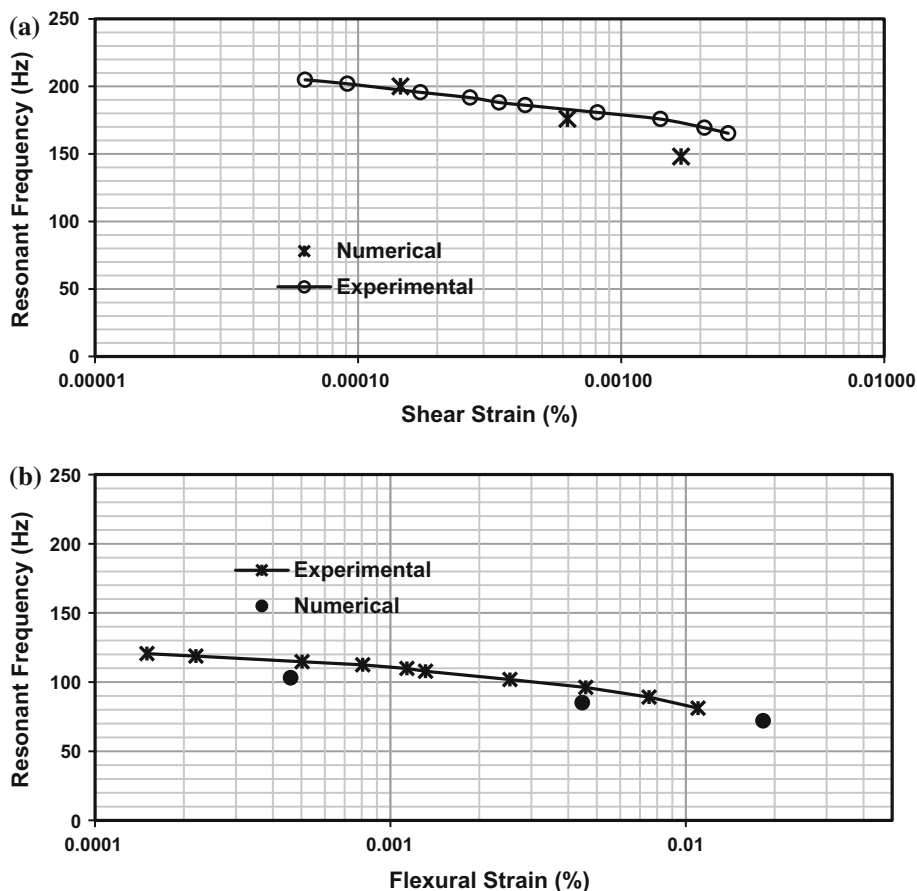
Fig. 14 **a** POP sample with two horizontal joints and **b** numerical simulation of sample with two joints

source. In most of the instances, these vibrations induce strain levels within the elastic range only. The long wavelength propagation of waves is a very general condition in rock mechanics due to the existence of closely spaced joints. The laboratory experiments conducted on

jointed samples using resonant column apparatus and numerical simulations describe the long wavelength propagation of waves across jointed rocks for a range of strain levels within the elastic limit. The wave velocities calculated from the resonant frequencies are a measure of the sample stiffness as shear and Young's moduli are obtained from these wave velocities. The variation of wave velocities with varying strain levels and stress conditions is an indication of the nonlinear behavior of rocks.

The resonant column tests on intact samples indicated that there is stiffness reduction with increasing strain levels, which is indicative of a dissipative medium and its nonlinear behavior. This may be due to the existence of voids, micro-cracks, etc., in the medium, representing the intact rocks. The numerical simulation of RC tests on jointed samples shows that the stiffness reduction of joints in addition to the stiffness reduction of material leads to the overall stiffness reduction of rock mass, while rock mass with inclined joints is stiffer than that with horizontal joints. The reduction in the joint stiffness (shear and normal) with increasing strain levels may be due to the decrease in the interlocking of asperities and contact area at the joints, with high amplitude of vibrations. The numerical

Fig. 15 Resonant frequency reduction across strain levels for sample with multiple horizontal joints **a** under torsional vibrations, **b** under flexural vibrations



simulations and experiments have proved that reduction in the joint spacing leads to the stiffness reduction of rock mass and increased the nonlinear elastic nature of rocks.

12 Conclusions

The nonlinear behavior of rocks is demonstrated in this paper with the help of resonant column tests conducted across a range of strain levels and using the numerical simulations. When the resonant column apparatus has its boundary condition as bottom fixed and top free with additional masses placed on the free end, the wavelength of the propagating wave calculated from the wave velocity and natural frequency is long and can attain the long wavelength condition. The resonant column tests using model material and the calculation of actual resonant frequencies from the obtained resonant frequencies are explained. The numerical simulation of resonant column tests on intact and jointed samples along with validation of the numerical model has been performed. The previous studies on long wavelength propagation of waves were constrained to a particular strain level,

whereas the present study demonstrates the strain-dependent wave propagation characteristics using numerical simulations. The numerical simulations have been used to show the nonlinear behavior of jointed rocks, and the joint stiffness that is obtained from the numerical simulations indicates that they are also strain dependent even within the elastic limit.

The conclusions that are drawn from the present study are:

- The nonlinear elastic behavior of rocks increases with increasing strain levels and with the inclusion of discontinuities.
- The shear stiffness of joint and normal stiffness of joint exhibit nonlinear behavior within the elastic limit.
- The behavior of jointed rock mass under torsional and flexural vibrations can be simulated using distinct element method.
- Reduction of normal and shear stiffness of joint with increasing strain levels leads to reduction of resonant frequencies, and in turn wave velocities and moduli of the rock mass.

Fig. 16 Resonant frequency reductions for samples with different number of joints under **a** torsional vibrations, **b** flexural vibrations

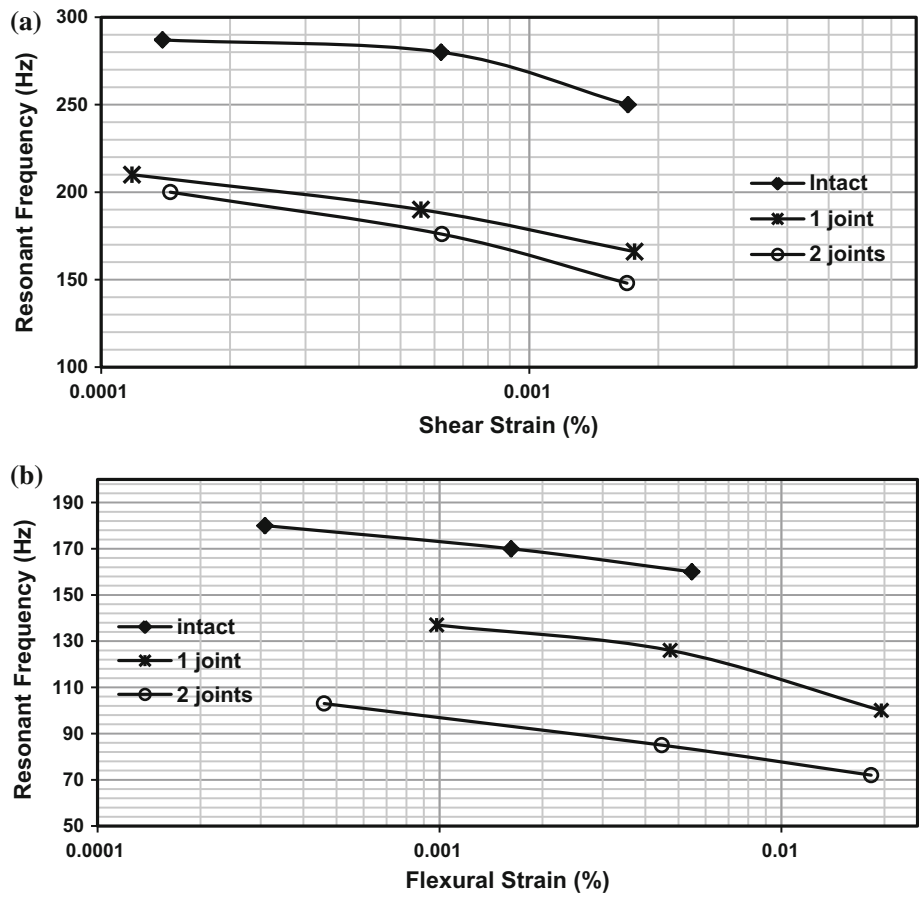


Fig. 17 **a** Numerical model of sample with four joints, **b** displacement contour obtained under torsional vibration, **c** stress contour obtained under torsional vibration, **d** displacement contour obtained under flexural vibration and **e** stress contour obtained under flexural vibration

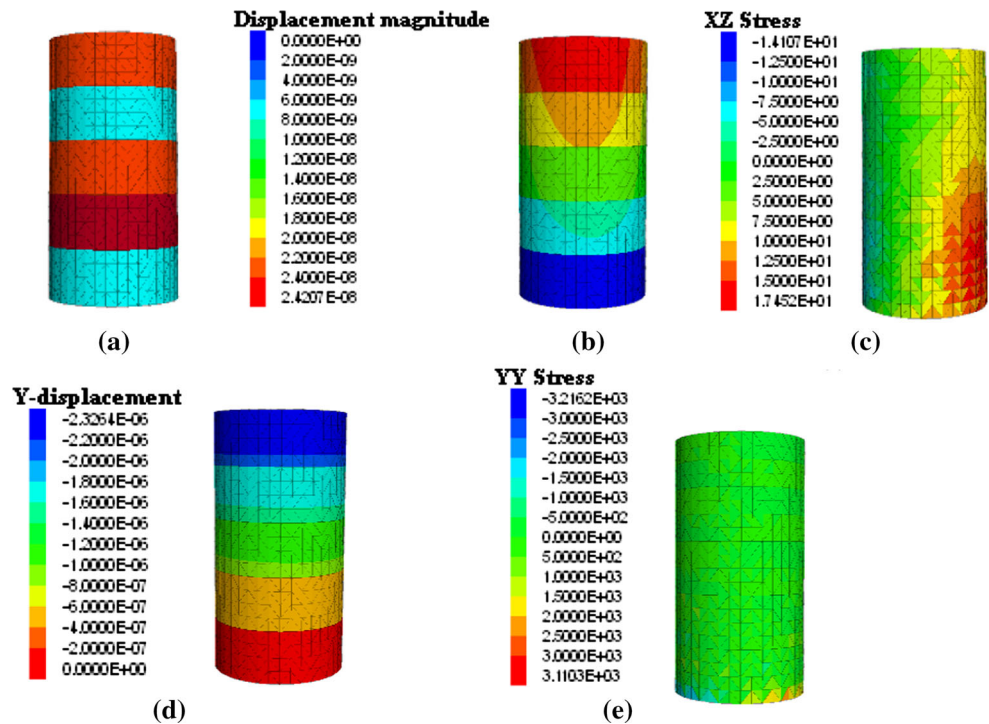


Table 2 Wave velocities calculated from the resonant frequencies obtained using numerical simulations

V_s (m/s)	Strain (%)	V_p (m/s)	Strain (%)
Sample—intact			
1349	1.39e−4	2235.5	3e−4
1316.5	6.2e−4	2111	1.6e−3
1175	1.7e−3	1987	5.47e−3
Sample—horizontal joint			
987	1.18e−4	1701	9.8e−4
893	5.58e−4	1565	4.7e−3
780.5	1.76e−3	1242	1.96e−2
Sample—inclined joint			
1091	1.3e−3	1614.5	1.18e−3
1076.7	5.2e−3	1552	4.6e−3
804	1.25e−2	1292	1.4e−2
Sample—two horizontal joints			
940	1.45e−4	1279	4.6e−4
827	6.25e−4	1055.6	4.5e−3
696	1.69e−3	894	1.8e−2

- Inclined joints have higher normal and shear stiffness and have higher wave velocities across them when compared to horizontal joints.
- The validated numerical model can be extended to studies involving more complex joint patterns and wave velocities across them can be obtained.

Acknowledgements The authors acknowledge the financial support of Ministry of Human Resource Development (MHRD), Government of India, in conducting the research.

References

- Barton N (2007) Rock quality, seismic velocity, attenuation and anisotropy. Taylor & Francis, London
- Bonner BP, Wanamaker BJ (1990) Nonlinear acoustic effects in rocks and soils. In: Thompson DO, Chimenti DE (eds) Review of progress in quantitative non destruction evaluation, vol 9. Plenum Press, New York, pp 1709–1713
- Cai JG, Zhao J (2000) Effects of multiple parallel fractures on apparent wave attenuation in rock masses. *Int J Rock Mech Min Sci* 37(4):661–682
- Cascante G, Santamarina C, Yassir N (1998) Flexural excitation in a standard torsional resonant column device. *Can Geotech J* 35:478–490
- Cha M, Cho G, Santamarina JC (2009) Long wavelength P-wave and S-wave propagation in jointed rock masses. *Geophysics* 74(5):E205–E214
- Deng XF, Zhu JB, Chen SG, Zhao J (2012) Some fundamental issues and verification of 3DEC in modeling wave propagation in jointed rock masses. *Rock Mech Rock Eng* 45(5):943–951
- Drnevich VP (1978) Resonant column testing-Problems and solutions. In: Silver M, Tiedemann D (eds) *Dynamic Geotechnical Testing*, STP35687S. ASTM International, West Conshohocken, PA, pp 384–398
- Fratta D, Santamarina JC (2002) Shear wave propagation in jointed rock: state of stress. *Geotechnique* 52(7):495–505
- ISRM (1978) International society for rock mechanics commission on standardization of laboratory and field tests. *Int J Rock Mech Min Sci Geomech Abstr* 15:319–368
- Johnson PA, Rasolofosaon PNJ (1996) Manifestation of nonlinear elasticity in rock: convincing evidence over large frequency and strain levels from laboratory studies. *Nonlinear Processes Geophys* 3:77–88
- Khan ZH, Cascante G, El-Naggar H (2008) Evaluation of the first mode of vibration and base fixidity in resonant column testing. *Geotech Test J ASTM* 31(1):1–11
- Kolsky H (1963) *Stress waves in solids*. Dover Publications, New York
- Kuhlemeyer RL, Lysmer J (1973) Finite element method accuracy for wave propagation problems. *J Soil Mech Found Div* 99:421–427
- Kumar J, Clayton CRI (2007) Effect of sample torsional stiffness on resonant column results. *Can Geotech J* 44:221–230
- Li Y, Wang J, Jung W, Ghassemi A (2012) Mechanical properties of intact rock and fractures in welded tuff from Newberry volcano. In: *Proceedings, thirty seventh workshop on geothermal reservoir engineering*, Stanford university, Stanford, California, SGP-TR-191
- Liu X (1994) *Nonlinear elasticity, seismic anisotropy and petrophysical properties of reservoir rocks*. Dissertation, Stanford University
- Mohd-Nordin MM, Song K, Cho G, Mohamed Z (2014) Long wavelength elastic wave propagation across naturally fractured rockmasses. *Rock Mech Rock Eng* 47(2):561–573
- Panchanathan S, Ramaswamy SV (1964) Skin friction between sand and construction materials. *J Indian Natl Soc Soil Mech Found Eng* 3(4):325–336
- Pande GN, Orlando A (2011) Computation of elastic stiffness of rock joints—a micromechanical approach. In: *Proceedings, international symposium on computational geomechanics*, Cavtat—Dubrovnik, Croatia
- Perino A (2011) *Wave propagation through discontinuous media in rock engineering*. Dissertation, Polytechnic University of Turin
- Perino A, Barla G (2015) Resonant column apparatus tests on intact and jointed rock specimens with numerical modeling validation. *Rock Mech Rock Eng* 48:197–211
- Potyondy JG (1961) Skin friction between various soils and construction materials. *Geotechnique* 11(4):339–353
- Richart FE Jr, Woods RD, Hall JR Jr (1970) *Vibrations of soils and foundations*. Prentice Hall, New Jersey
- Rosso RS (1976) A comparison of joint stiffness measurements in direct shear, triaxial compression and in situ. *Int J Rock Mech Min Sci Geomech Abstr* 13:167–172
- Schoenberg M, Muir F (1989) A calculus for finely layered anisotropic media. *Geophysics* 54:581–589
- Schoenberg M, Sayers CM (1995) Seismic anisotropy of fractured rock. *Geophysics* 60:204–211
- Sebastian R, Sitharam TG (2015) Long wavelength propagation of elastic waves across frictional and filled rock joints with different orientations: experimental results. *Geotech Geol Eng* 33:923–934
- Sebastian R, Sitharam TG (2016) Long wavelength propagation of waves in jointed rocks using resonant column experiments and model material. *Geomech Geoeng Int J* 11(4):281–296
- Siggins AF (1993) Dynamic elastic tests for rock engineering. In: Hudson JA et al (eds) *Comprehensive rock engineering*, vol 3. Pergamon, London, pp 601–618
- Sitharam TG, Resmi S (2017) Numerical simulation of resonant column tests on jointed rocks using DEM. In: Li X, Feng Y,

- Mustoe G (eds) Proceedings of the 7th international conference on discrete element methods. Springer, Singapore, pp 889–896
- Thomsen L (1990) Poisson was not a geophysicist. *Lead Edge* 9(12):27–29
- Thomsen L (1996) Poisson was not a rock physicist either. *Lead Edge* 15(7):852–855
- Winkler K, Nur A (1979) Pore fluids and seismic attenuation in rocks. *Geophys Res Lett* 6:1–4